Development and Analysis of a Homopolar Consequent Pole Transverse Flux Magnetic Gear

Salek A. Khan
Dept. of Electrical & Computer Engineering
University of Texas at Dallas
Richardson, Texas, United States
salek@utdallas.edu

Matthew C. Gardner
Dept. of Electrical & Computer Engineering
University of Texas at Dallas
Richardson, Texas, United States
matthew.gardner@utdallas.edu

***Abstract*—Magnetic gears perform the same function as mechanical gears but rely on noncontact operation to transfer power, producing many potential advantages over mechanical gears. This paper proposes two new topologies of transverse flux magnetic gear (TFMG). The new topologies are parametrically evaluated using 3D finite element analysis (FEA). The homopolar consequent pole TFMG offers simple assembly with only a single magnet but suffers from a low volumetric torque density (VTD) based on preliminary studies and a proof-of-concept prototype. The doubly magnetized consequent pole TFMG requires more magnets but could produce a higher VTD, but that VTD is still relatively low for a coaxial magnetic gear. A prototype of the homopolar consequent pole TFMG gear was built. Its measured slip torque agreed well with simulations, but it experienced relatively significant bearing losses. Although the VTD of this new topology is low, its simplicity with only a single permanent magnet could be advantageous for small-torque applications where manufacturing complexity can drive cost.**

***Keywords*—Finite-element analysis (FEA), homopolar, magnetic gear, permanent magnet, torque density, torque ripple, transverse flux.**

I. Introduction

The main disadvantages of traditional mechanical gears result from the mechanical contact between teeth. This contact leads to premature wear, friction, increased maintenance requirements, and reduced reliability. However, magnetic gears employ modulated magnetic fields, instead of mechanical contact, to transfer power from one gear to another. This noncontact mode of operation provides many potential advantages, including physical isolation between the shafts, increased efficiency, improved reliability, reduced acoustic noise, and the ability to transfer torque through solid boundaries. Thus, magnetic gears have been proposed for a wide range of applications, including electric vehicles [1], [2], wind turbines [3], [4], ocean wave energy harvesting [5], [6], and ships [7], [8]. Research in the field has developed a few different topologies of magnetic gears, each with its own advantages and disadvantages.

The most heavily researched topology is the radial flux magnetic gear (RFMG) [1]-[9]. RFMGs have two coaxial rotors with permanent magnets (PMs) magnetized in the radial direction (Rotors 1 and 3) and a ring of ferromagnetic modulators (Rotor 2) in between the PM rotors, as shown in Fig. 1(a). Although RFMGs are the most common, there are also other coaxial topologies, such as axial flux magnetic gears (AFMGs) [9], [10] and transverse flux magnetic gears (TFMGs) [11], [12]. AFMGs have two disks with axially magnetized PMs and have a ring of ferromagnetic modulators between the two disks, as shown in Fig. 1(b). TFMGs typically have two rotors with radially magnetized PMs axially separated by a gap with the modulators radially beyond the PM rotors, as shown in Fig. 1(c). RFMGs have demonstrated the highest torque densities in terms of active material mass, whereas AFMGs are particularly suitable for applications requiring a "pancake" form factor [9]. While TFMGs suffer from significant leakage flux [11] and have anecdotally demonstrated lower torque densities than RFMGs and AFMGs [12], [13], they have the advantage of easier assembly because the modulators are not between the PM rotors [12].

In this paper, two new TFMG topologies are proposed, their parameters are varied to characterize the torque density, and a prototype of one of the topologies is built and tested. In the homopolar consequent pole topology (HCPT), the radially magnetized PMs are replaced by ferromagnetic teeth, and an axially magnetized PM disk is placed in the central gap between the rotors, as shown in Fig. 1(d). The main advantage of this new proposed topology is simpler assembly, as there is only one PM, which could potentially be magnetized after the design is already assembled. The second proposed topology, the doubly magnetized consequent pole topology (DMCPT), is very similar to the HCPT however, the gaps between the teeth of the gears have been filled in with radially magnetized PMs, as shown in Fig. 1(e). Although this design will be more challenging to assemble than the HCPT, it may still be easier to manufacturer than the conventional TFMGs because the magnets can potentially be held in place by the teeth without the need for a sleeve as in [14], and it can produce more torque than the HCPT due to the added PMs. In the RFMG, AFMG, and traditional TFMG topologies, manufacturing becomes complex due to two main factors. The first is the placement and positioning of many small PMs. Any misalignment of the PMs can degrade the performance of the gear. Secondly, for

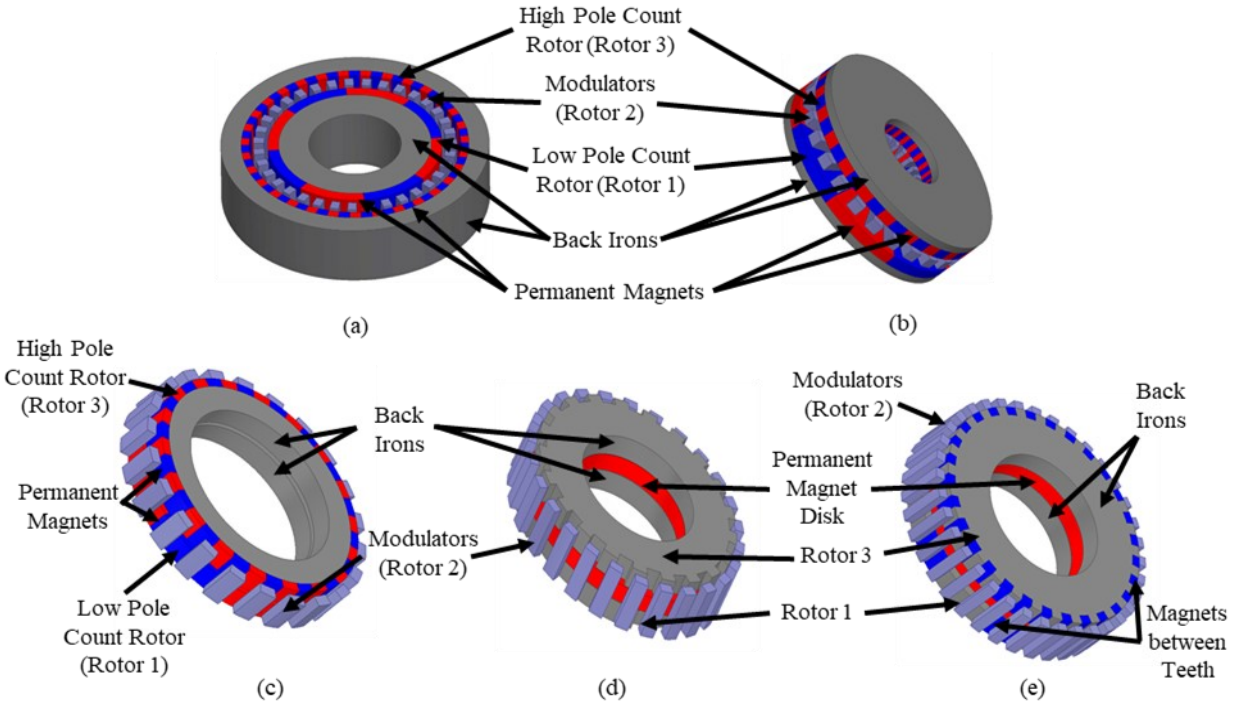

Fig. 1: (a) Radial flux magnetic gear, (b) axial flux magnetic gear, (c) conventional transverse flux magnetic gear, (d) HCPT, and (e) DMCPT

the RFMG and AFMG, the modulators are held between the rotors, which requires difficult to manufacture brackets/support structures [15], [16]. The proposed HCPT topology will solve both these issues by using a single magnetic disk (reducing the magnet count to one), and modulator pieces held around the moving rotors.

For each of these coaxial magnetic gear topologies, the number of modulators (Q_2) for optimal operation is determined by the Rotor 1 and Rotor 3 pole counts according to

$$Q_2 = P_1 + P_3, \tag{1}$$

where P_1 and P_3 are the number of pole pairs or, in the case of the proposed TFMGs, salient teeth on Rotors 1 and 3, respectively. Then, the gear ratio (G) with Rotor 2 fixed is given by

$$G|_{\omega_2=0} = \frac{\omega_1}{\omega_3} = \frac{-P_3}{P_1}, \tag{2}$$

where ω_1, ω_2, and ω_3 represent the angular speeds of Rotors 1, 2, and 3, respectively. Alternatively, Rotor 3 can be fixed, which leads to a gear ratio between Rotors 1 and 2 that is positive and larger in magnitude than the gear ratio in (2) by unity. However, for TFMGs it is likely more practical to fix Rotor 2.

II. Operating Principle

Figs. 2 – 7 illustrate the flux densities in an example design of the HCPT. In Fig. 4, the magnetic flux can be seen traveling axially through the axially magnetized PM disk, through Rotor 3 to a modulator, axially through the modulator, and lastly through Rotor 1 back to the PM disk.

For this example design, the Rotor 1 and 3 teeth are becoming saturated. Additionally, near the top and bottom edges of the modulator, some fringing flux can be seen. Fig. 5(a) shows the flux density distribution from a different cross-sectional view. The areas between the Rotor 1 teeth have very little flux passing through them, resulting in a significant $P_1 = 3$ harmonic in the airgap, as shown in Fig. 6. Additionally, flux can be seen in the modulators that are fully or partially adjacent to a tooth on Rotor 1, while modulators that are not near a tooth have considerably less flux passing through them.

Fig. 5(b) shows the flux distribution in Rotor 3. As in Fig. 5(a), the areas between rotor teeth have significantly less flux passing through them than the teeth themselves. The most flux flows from the rotor to the modulator when a tooth tip is fully aligned with the face of the modulator piece. When a tooth is between modulators, the flux path is split between the nearest modulators. Due to the higher number of teeth on Rotor 3, when a modulator is exactly between rotor teeth, there is still some flux in the modulator due to leakage flux. Fig. 7 shows the radial flux density in the air gap between Rotor 3 and the modulators; both $P_1 = 3$ and $P_3 = 11$ harmonics are clearly visible, as well as a $Q_2 = 14$ harmonic.

As seen in this section, the HCPT operates in a unique way by utilizing a singular axially magnetized magnet. This overall lower part count design in combination with the use of a single PM could allow the HCPT to be ideal for minimizing manufacturing and assembly costs.

III. Design Study

Each feasible design parameter combination in Table I was evaluated for both topologies using 3D finite element analysis (FEA). For P_1 values of 3, 5, and 7, P_3 values of 11,

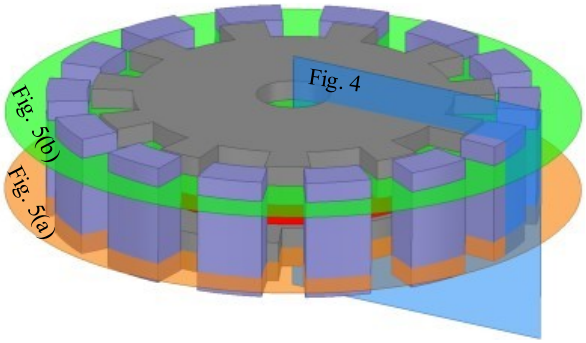

Fig. 2: Planes on which Fig. 4, and Fig. 5 were plotted.

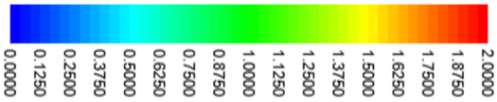

Fig. 3: Legend for flux density in Tesla for Figs. 4 and 5.

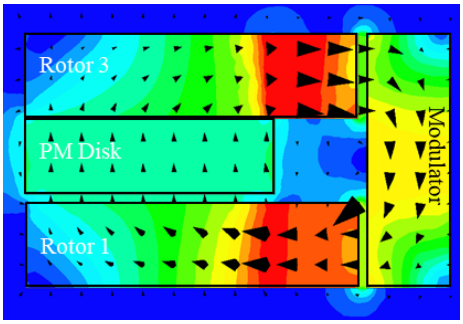

Fig. 4: Side cross-section view of the HCPT showing the magnetic flux density and corresponding vectors.

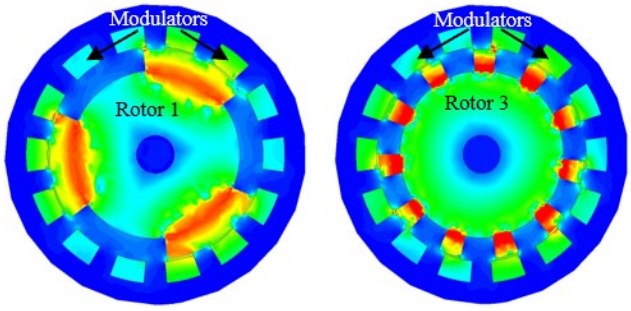

(a) (b)

Fig. 5: Top cross-section view of the HCPT showing the magnetic flux and modulators and (a) Rotor 1 and (b) Rotor 3.

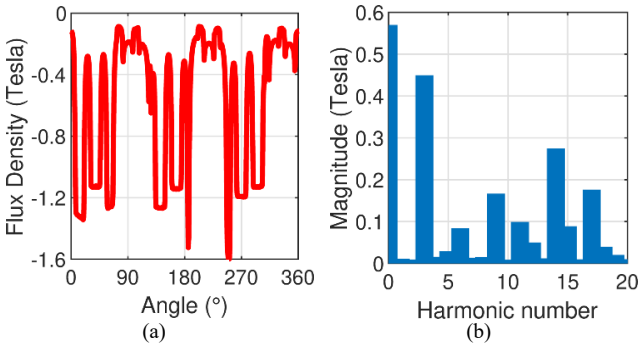

(a) (b)

Fig. 6: (a) Radial flux density in airgap between Rotor 1 and modulators and (b) harmonic components

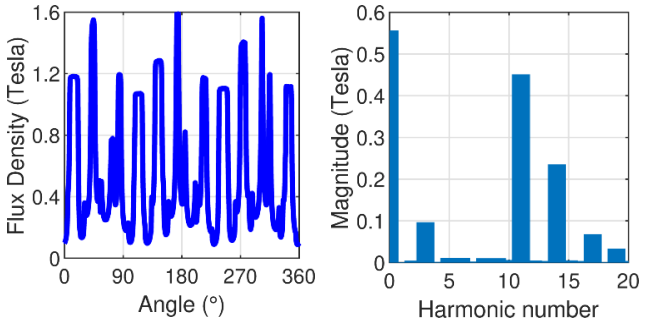

(a) (b)

Fig. 7: (a) Radial flux density in airgap between Rotor 3 and modulators and (b) harmonic components

17, and 23 were used, respectively, to yield non-integer (to reduce torque ripple [8]) gear ratios between 3 and 4. Although a lower P_1 value produced higher torque, as shown in Fig. 8, the lowest value that was used for P_1 was 3, since a gear with fewer than 3 teeth would experience large torque ripples [8], [17].

Magnetic gears are often compared using volumetric torque density (VTD), which provides a normalized value for the compactness of the design. The VTD of a magnetic gear is given by the slip torque of the low-speed rotor (Rotor 3, in this case) divided by the active volume, which is the volume of the smallest cylinder enclosing all the active components (magnets, modulators, rotor back irons, and teeth) and does not include any housings, brackets, bearings, etc. For the design combinations summarized by Table I, the HCPT is able to achieve a VTD up to 6.5 kNm/m^3, whereas the DMCPT is able to achieve a VTD up to 26.1 kNm/m^3. Thus, by simply adding magnets between the teeth of the HCPT, the DMCPT is able to achieve a significantly larger VTD.

IV. Data Trends

Fig. 9 illustrates the relationship between H_{PM} and VTD. As H_{PM} increases, there is a tradeoff between increasing the PM mass in the design, which tends to increase torque, and increasing the axial length of the modulators, which increases flux leakage [11] and, thus, reduces torque. With higher pole counts, the gap between adjacent modulators becomes narrower, making the impacts of flux leakage more significant, so the higher P_1 cases tend to favor smaller H_{PM} values.

Fig. 10 illustrates how O_{Mod} affects the achievable VTD. In the model, O_{Mod} determined the axial length of the overlap for the modulators with each of Rotors 1 and 3. The optimal overlap values are also dependent on the H_R value, as it directly determines what the largest possible value of O_{Mod} is. The corresponding H_R value for each of the points shown in Figs. 10(a) and (b) is shown in Figs. 10 (c) and (d), respectively. For the HCPT, going from a O_{Mod} value of 5 mm to a value of 10 mm increased the VTD since with larger overlap reduces the air gap reluctance for the traveling flux. However, the VTD was reduced as O_{Mod} increased beyond 10

mm because the larger H_R increased the gear volume. When going from an O_{Mod} value of 15 mm to a value of 20 mm, the VTD was reduced due to increased leakage flux between modulators. For the DMCPT, the trend is clearer, as the overlap amount is increased, the resulting VTD is also generally higher up to 15 mm of overlap. However, due to increased leakage flux, increasing O_{Mod} from 15 mm to 20 mm slightly reduces the torque. Thus, both the HCPT and DMCPT prefer values within a few mm of a full overlap.

TABLE I. SUMMARY OF SIMULATED PARAMETERS FOR THE HCPT AND DMCPT

Symbol	Description	Values
T_{BI}	Radial thickness of rotor back irons	30, 40 mm
T_{GT}	Radial thickness of teeth	10, 15 mm
T_{Mod}	Radial thickness of modulators	5, 10 mm
R_{Out}	Outer radius of modulators	100 mm
H_{PM}	Axial height of axially magnetized PM disk	3, 6, 9, 12 mm
H_R	Axial height of Rotors 1 and 3	5, 10, 20 mm
α_{Mod}	Angular fill factor of modulators	0.4, 0.5, 0.6
α_{T1}	Angular fill factor of teeth on Rotor 1	0.4, 0.5
α_{T3}	Angular fill factor of teeth on Rotor 3	0.4, 0.5
O_{Mod}	Axial overlap between modulators and Rotors 1 and 3	5, 10, 15, 20 mm
A_A	Axial air gap	1 mm
A_R	Radial air gap	1 mm
P_1	Number of teeth on Rotor 1	3, 5, 7

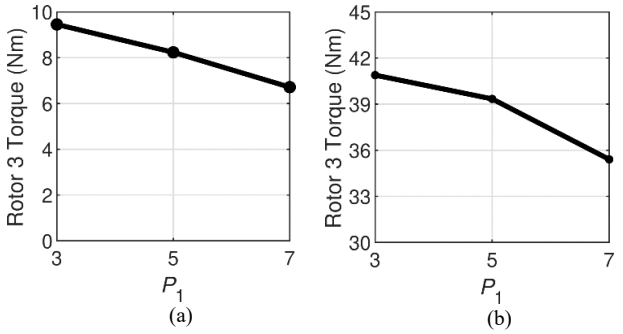

Fig. 8: Maximum achievable Rotor 3 slip torque plotted against P_1 for the (a) HCPT and (b) DMCPT

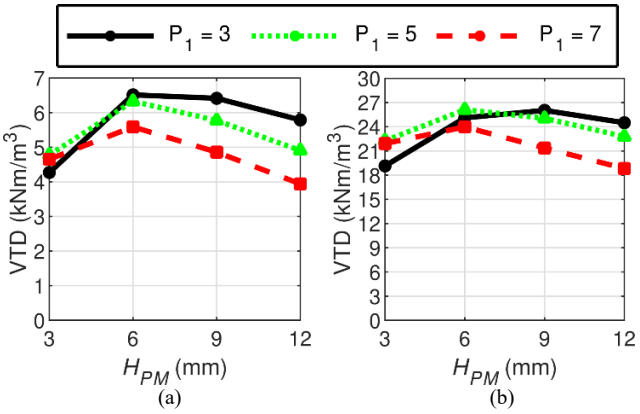

Fig. 9: Maximum achievable VTD plotted against H_{PM} for the (a) HCPT and (b) DMCPT for different pole counts.

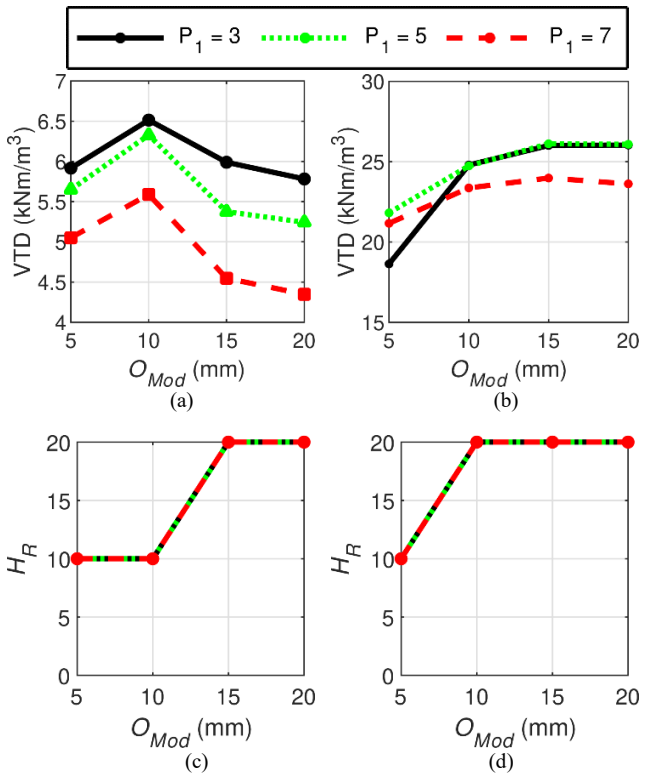

Fig. 10: Maximum achievable VTD plotted against O_{Mod} for the (a) HCPT and (b) DMCPT for different pole counts. The corresponding H_R values for the maximum VTD (c) HCPT and (d) DMCPT designs.

Reducing the overlap can increase the air gap reluctance for flux traveling between Rotors 1 or 3 and the modulators, but reducing the overlap also reduces the axial length of the modulators, which reduces the tangential leakage flux between adjacent modulators.

Fig. 11 illustrates how α_{Mod}, α_{T1}, and α_{T3} affect VTD. Each fill factor, α, is a coefficient that controls the angular width of a specific feature on the gear, a higher fill factor represents a tangentially wider component, and a lower fill factor represents a narrower component. For the HCPT, VTD is maximized with a α_{Mod} and Rotor 1 and Rotor 3 fill factors of at least 0.5. Similarly, for DMCPT the optimal value for α_{Mod} is at least 0.5; however, the optimal α_{T1} and α_{T3} values are less than 0.5. A larger modulator fill factor enables the modulators to carry more flux, at the expense of increased leakage flux. Likewise, a larger rotor tooth fill factor in the HCPT allows for more flux to travel through the teeth. In the DMCPT, the smaller tooth fill factors allow for higher magnet volume, which increases VTD.

V. PROTOTYPE DESIGN

The parameters in Table II were chosen to design and build a prototype of the AMPCT. These values were selected to balance performance with manufacturing feasibility and cost. For the physical prototype, R_{Out} was constrained to 60 mm to simplify fabrication from off-the-shelf soft magnetic

TABLE II. CHOSEN VALUES FOR AMPCT PROTOTYPE DESIGN

Symbol	Value	Symbol	Value
T_{BI}	20 mm	α_{T1}	0.4
T_{GT}	10 mm	α_{T3}	0.4
T_{Mod}	10 mm	O_{Mod}	15 mm
R_{Out}	60 mm	P_1	3
H_{PM}	9 mm	A_A	3 mm
H_R	20 mm	A_R	1 mm
α_{Mod}	0.6	G	11:3 = 3.67:1

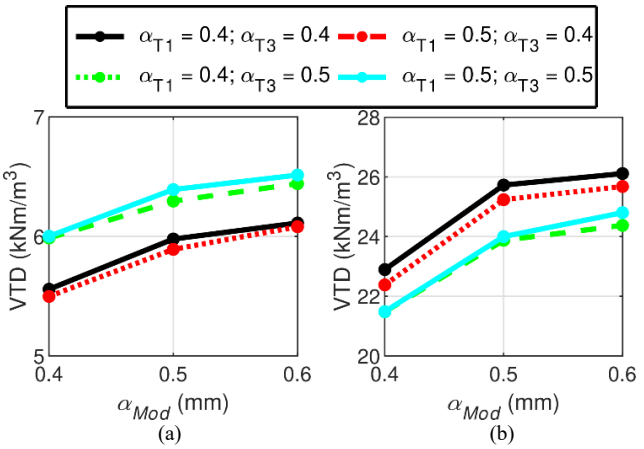

Fig. 11: Maximum achievable VTD plotted against α_{Mod} for the (a) HCPT and (b) DMCPT for different tooth fill factors.

composite (Somaloy) pucks.

There were two main complexities in designing a physical prototype of the AMPCT: the axial pulling force of the large permanent magnet disk and the positioning of the modulators. The simulation data predicted that a 3 mm axial air gap between the permanent magnet and the Rotor 3 would yield an axial force of 640 N.

To position the modulators in a ring, as shown in Fig. 1(d), a modulator "cage" was designed that would house the modulators in the correct position while not interfering with the flow of the magnetic flux. The cage was additively manufactured from PETG, as shown in Fig. 12(a).

Another advantage of the TFMG topologies is that modulator thickness can be increased (either to increase mechanical strength or to accommodate more magnetic flux) without increasing the distance between the rotors. This freedom in design can prevent the modulators from cracking [18] or experiencing large deflections [19] during operation.

The end caps were additively manufactured from PETG. However, the rotors had to be magnetically permeable, so we had to resort to traditional machining. The rotors and modulators were made of a soft magnetic composite, Somaloy [20], as illustrated in Fig. 12(b). Each modulator was fabricated from two pieces (because the modulators were designed with an axial length of 40 mm, but the available Somaloy pucks only had an axial length of 20 mm), and once they were in the modulator cage, the two halves were forced together via the end caps.

Since one of the design goals was to reduce the torque ripple in the gear, simulations were run to determine if

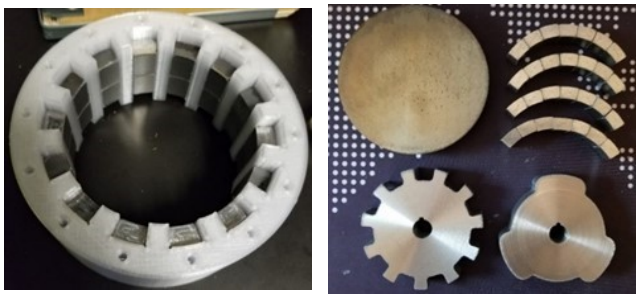

Fig. 12: (a) The 3D printed modulator cage with the modulator pieces inserted and (b) a raw Somaloy puck (top left), the 28 "half" modulators (top right), Rotor 3 (bottom left), and Rotor 1 (bottom right).

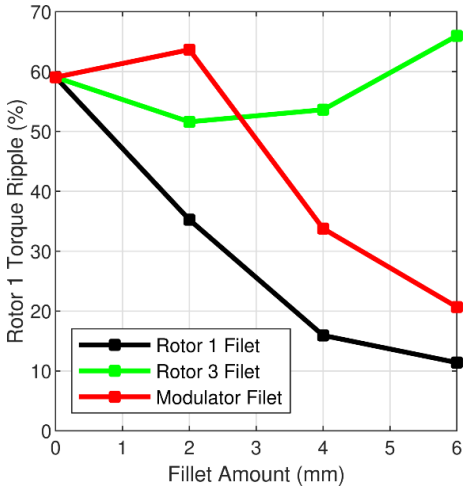

Fig. 13: The torque ripple on Rotor 1 versus various fillet amounts on Rotor 1, Rotor 3, and the modulators.

fileting or chamfering the rotor teeth or modulators on the edges adjacent to the air gap would reduce the torque ripple in the gear. The results of the simulations can be seen in Fig. 13, which shows the impact on the Rotor 1 torque ripple (which is generally much more significant than the Rotor 3 torque ripple [8]) of fileting each SMC component in the prototype design.

Increasing the filet size on the Rotor 1 teeth or the modulators generally reduces the Rotor 1 torque ripple, whereas increasing the filet on the Rotor 3 teeth generally has little impact on the Rotor 1 torque ripple but reduces the average torque. However, these trends for the Rotor 3 teeth and modulators are not completely smooth because average torque decreases significantly as the filet size increases, so the ripple becomes a larger percentage of the torque.

After considering the results from the simulations, we chose a 9 mm filet on the Rotor 1 teeth and no filet modifications to Rotor 3 or the modulators because this yielded significant torque ripple reduction with a minimal sacrifice in average torque. Additionally, to make machining easier, the internal 90-degree corners of the teeth on Rotors 1 and 3 were fileted.

A simulation verified that this did not negatively affect the torque ripple or the torque output. The fillets can be seen in Fig. 12. The final gear design is shown in Fig. 14.

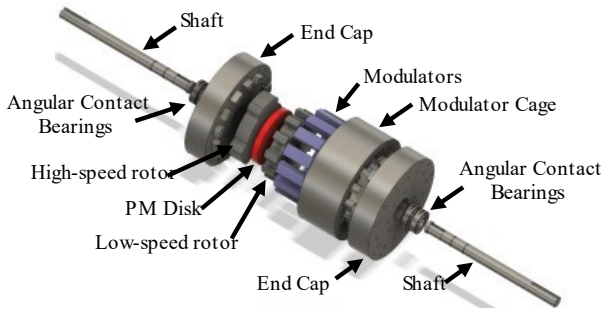

Fig. 14: The final design of the AMCPT prototype.

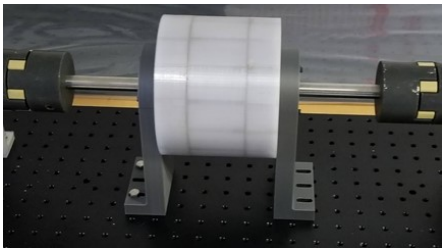

Fig. 15: The assembled HCPT prototype.

VI. Prototype Assembly

As mentioned previously, the main difficulty with assembling the HCPT topology is positioning Rotors 1 and 3 in a controlled manner, given the large magnetic attraction force the permanent magnet disk creates. However, it is important to note that with a properly designed HCPT gear, this is the only difficult step. Furthermore, since the proposed topology only uses one magnet, the manufacturing can be less time consuming than other magnetic gear topologies, such as the RFMG or AFMG. Additionally, it may be possible to magnetize the permanent magnet after the gear has been partially or fully assembled, which would eliminate the main difficulty in assembling the magnetic gear.

The assembly of the prototype started by first additively manufacturing the two end caps and the modulator cage. These pieces were made from an engineering grade PETG plastic at 80% infill to maximize strength. Additionally, two angular contact bearings were used in each end cap to support the axial forces on the shafts. The rotors were press fit and keyed onto the shafts, then the modulators were pressed into the modulator cage, and finally the two halves of the gear were mated together. The final assembled HCPT gear can be seen in Fig. 15.

VII. Experimental Results

There are two main parameters that were measured with the HCPT prototype. The first parameter is the slip torque of the gear. This is useful to determine the maximum load the gear can drive without slipping. To measure the slip torque, both ends of the prototype were connected to torque meters. One end of the prototype was locked in place, while the other end was rotated until slippage occurred. The signal registered

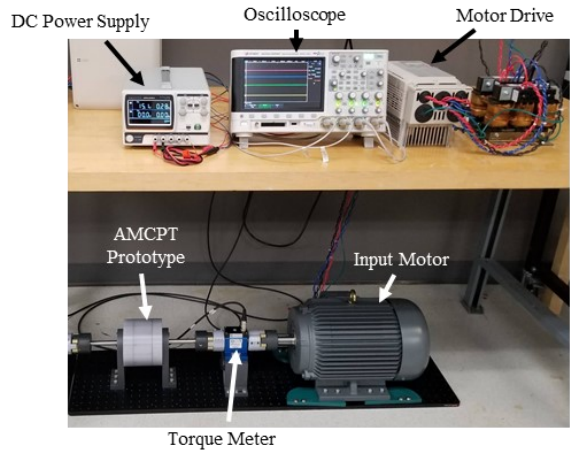

Fig. 16: No load loss test setup.

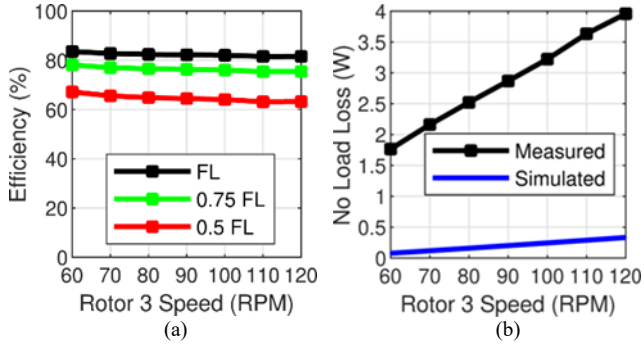

Fig. 17: (a) Projected efficiency of the HCPT at different load conditions based on the measured no-load losses and (b) the measured no load losses and simulated electromagnetic no-load loss of the HCPT prototype.

by the locked torque meter was measured by an oscilloscope. The Rotor 3 slip torque was measured in both the forwards and reverse directions, and the average value was 1.71 Nm, which is 4.9% higher than the simulated 1.63 Nm slip torque. The most likely explanation for the discrepancy between the simulations and the measurement is that the axial airgap in the prototype did not precisely match the simulated model.

The second parameter of interest was the prototype's efficiency. However, due to the small torques on the high-speed side, it was difficult to obtain adequately precise efficiency measurements under load. Instead, the gear was tested under a no-load condition with a motor driving the low-speed rotor, to find the losses. Then the efficiency could be projected for full load (FL), 75%, and 50% of FL conditions, assuming the losses do not vary with load, as in [6] and [21]. The measurement setup for measuring no-load losses can be seen in Fig. 16, and the measured no-load loss and projected efficiency data can be seen in Figs. 17. At maximum load the HCPT reached a peak projected efficiency of 83%. This disappointing number is likely due to high friction, resulting from the axial forces on the bearings because the simulated electromagnetic losses were relatively small, as shown in Fig.17(b).

Somaloy, a soft magnetic composite, was used for the rotors and modulators to avoid inducing significant eddy

currents from the 3D flux paths in the gear and to provide isotropic permeability. It is important to note that the use of Somaloy for the rotors and modulators did not significantly degrade the torque. To verify this, identical simulations were run, with the only difference being that in one model the rotors and modulators are made of Somaloy, whereas they are made from 1010 steel in the other model. The Somaloy gear had a simulated slip torque of 1.63 Nm while the 1010 steel gear had a slip torque of 1.67 Nm. This represents a 2.4% difference, which indicates that torque is not significantly reduced by using Somaloy, at least for the prototyped design.

VIII. Conclusion

This paper introduces and evaluates two different TFMG topologies. The HCPT achieved poor VTDs; however, its assembly is simpler than other types of magnetic gears, due to its utilization of a single large magnet, which could potentially be magnetized after assembly, rather than many smaller magnets and due to the location of the modulators radially beyond Rotors 1 and 3. On the other hand, the DMCPT was able to produce a much higher VTD that was about four times greater than that of the HCPT. While the DMCPT's torque density is still lower than many magnetic gear topologies, it should also be easier to fabricate than many conventional magnetic gear topologies, due to its modulator placement and because the teeth can be used to align the magnets. A prototype HCPT validated the simulated slip torques but had significant bearing losses, likely due to axial forces. Ultimately, the HCPT and DMCPT may be most suitable for small, cost-sensitive applications requiring noncontact torque transmission, where their reduced manufacturing complexity relative to conventional magnetic gears may outweigh their disadvantages.

References

[1] T. V. Frandsen et al., "Motor integrated permanent magnet gear in a battery electrical vehicle," *IEEE Trans. Ind. Appl.*, vol. 51, no. 2, pp. 1516-1525, Mar.-Apr. 2015.

[2] P. Chmelicek, S. D. Calverley, R. S. Dragan, and K. Atallah, "Dual rotor magnetically geared power split device for hybrid electric vehicles," *IEEE Trans. Ind. Appl.*, vol. 55, no. 2, pp. 1484-1494, Mar.-Apr. 2019.

[3] M. Desvaux, R. L. G. Latimier, B. Multon, H. B. Ahmed, and S. Sire, "Design and optimization of magnetic gears with arrangement and mechanical constraints for wind turbine applications," in *Proc. Int. Conf. Ecological Veh. Renewable Energies*, 2016, pp. 1-8.

[4] L. Jian, K. T. Chau, and J. Z. Jiang, "A magnetic-geared outer-rotor permanent-magnet brushless machine for wind power generation," *IEEE Trans. Ind. Appl.*, vol. 45, no. 3, pp. 954–962, May-Jun. 2009.

[5] K. K. Uppalapati, J. Z. Bird, D. Jia, J. Garner, and A. Zhou, "Performance of a magnetic gear using ferrite magnets for low speed ocean power generation," in *Proc. IEEE Energy Convers. Congr. Expo.*, 2012, pp. 3348– 3355.

[6] M. Johnson, M. C. Gardner, H. A. Toliyat, S. Englebretson, W. Ouyang, and C. Tschida, "Design, Construction, and Analysis of a Large-Scale Inner Stator Radial Flux Magnetically Geared Generator for Wave Energy Conversion," *IEEE Trans. Ind. Appl.*, vol. 54, no. 4, pp. 3305-3314, Jul.-Aug. 2018.

[7] L. MacNeil, B. Claus, and R. Bachmayer, "Design and evaluation of a magnetically-geared underwater propulsion system for autonomous underwater and surface craft," in *Proc. Int. Conf. IEEE Oceans*, 2014, pp. 1-8.

[8] N. W. Frank and H. A. Toliyat, "Gearing ratios of a magnetic gear for marine applications," in *Proc. IEEE Elect. Ship Technol. Symp.*, 2009, pp. 477–481.

[9] M. C. Gardner, M. Johnson, and H. A. Toliyat, "Comparison of Surface Permanent Magnet Axial and Radial Flux Coaxial Magnetic Gears," *IEEE Trans. Energy Convers.*, vol. 33, no. 4, pp. 2250-2259, Dec. 2018.

[10] M. Johnson, A. Shapoury, P. Boghrat, M. Post, and H. A. Toliyat, "Analysis and development of an axial flux magnetic gear," in *Proc. IEEE Energy Convers. Congr. Expo.*, 2014, pp. 5893-5900.

[11] X. Li, S. Liu, Y. Wang, and Y. Fan, "Investigation of the flux leakage effects in transverse-flux magnetic gear," in *Proc. Int. Conf. Elect. Mach. Syst.*, 2017, pp. 1-5.

[12] W. Bomela, J. Z. Bird, and V. M. Acharya, "The Performance of a Transverse Flux Magnetic Gear," *IEEE Trans. Mag.*, vol. 50, no. 1, pp. 1-4, Jan. 2014.

[13] Y. Chen, W. N. Fu, S. L. Ho, and H. Liu, "A Quantitative Comparison Analysis of Radial-Flux, Transverse-Flux, and Axial-Flux Magnetic Gears," *IEEE Trans. Mag.*, vol. 50, no. 11, pp. 1-4, Nov. 2014.

[14] M. Johnson, S. Hasanpour, M. C. Gardner, and H. A. Toliyat, "Analysis and Benchmarking of Radial Flux Cycloidal Magnetic Gears with Reduced Permanent Magnet Piece Count Using Consequent Poles", in *Proc. IEEE Energy Convers. Congr. Expo*, 2021, pp. 1-8.

[15] S. A. Khan, G. Duan, and M. C. Gardner, "Comparison of Modulator Retention Shapes for Radial Flux Coaxial Magnetic Gears", in Proc. IEEE Energy Convers. Congr. Expo, 2022, pp. 1-7.

[16] T. F. Tallerico, Z. A. Cameron and J. J. Scheidler, "Design of a Magnetic Gear for NASA's Vertical Lift Quadrotor Concept Vehicle," 2019 AIAA/IEEE Electric Aircraft Technologies Symposium (EATS), pp. 1-2, Aug. 2019.

[17] B. Praslicka, M. C. Gardner, M. Johnson, and H. A. Toliyat, "Review and Analysis of Coaxial Magnetic Gear Pole Pair Count Selection Effects," *IEEE Trans. Emerg. Sel. Topics Power Electron.*, early access, doi: 10.1109/JESTPE.2021.3053544.

[18] T. Tallerico, J. Scheidler, Z. Cameron, "Magnetic Gears and Their Structural Limitations" [PowerPoint slides]. NASA. https://ntrs.nasa.gov/api/citations/20190032274/downloads/20190032274.pdf

[19] K. K. Uppalapati and J. Z. Bird, "An Iterative Magnetomechanical Deflection Model for a Magnetic Gear," *IEEE Trans. Mag*,, vol. 50, no. 2, pp. 245-248, Feb. 2014.

[20] Höganäs AB, "Somaloy 3P Material Data", Feb. 2016, https://www.hoganas.com/globalassets/download-media/sharepoint/brochures-and-datasheets---all-documents/somaloy_somaloy-3p-material-data_2273hog.pdf

[21] M. Fukuoka, K. Nakamura, and O. Ichinokura, "Experimental tests of surface permanent magnet magnetic gear," in *Proc. IEEE Int. Conf. Elect. Mach. and Systems*, 2012, pp. 1-6.

Salek A. Khan (S' 21) earned his B.S. in electrical engineering from the University of Texas at Dallas in 2021. He is currently pursuing a doctoral degree in electrical engineering. His research interests include the design and analysis of magnetic gears.

Matthew C. Gardner (S' 15, M' 19) earned his B.S. in electrical engineering from Baylor University, Waco, Texas in 2014. He earned his Ph.D. in electrical engineering from Texas A&M University, College Station, Texas in 2019. In August 2020, he joined the University of Texas at Dallas, where he is an assistant professor. His research interests include optimal design and control of electric machines and magnetic gears.